The influence of multidirectional leakage flux on transformer core losses

Wei Wang[1], Arne Nysveen[1], Niklas Magnusson[2]

[1]Norwegian University of Science and Technology, Trondheim, NO-7491 Norway, weiwan@ntnu.no
[2]SINTEF Energy Research, NO-7465 Trondheim, Norway

***Abstract*—In a power transformer, the leakage flux enters the laminations of the iron core in different directions. Depending on the orientation of the leakage flux, it can add eddy current and hysteresis losses to the well-documented losses caused by the main flux. To study the principles of the influence of the leakage flux on the losses in transformer cores, the problem was isolated to an experiment on a stack of laminations in an Epstein-like frame. The frame carried the main flux, while artificial leakage flux is created and forced to enter the laminations in the two directions perpendicular to the main flux. Additionally, the system was modelled using finite elements to interpret the physical phenomena. The results revealed that the loading conditions have a significant impact on the local eddy current loss and on the overall power loss. The identified additional magnetic losses show that under inductive loading, conventional no-load tests can underestimate the core losses considerably.**

***Index Terms*—Eddy current; Lamination; Magnetic anisotropy; Magnetic flux leakage; Magnetic losses; Power transformer.**

I. Introduction

RENEWABLE energy and heavy industries introduce more variable load patterns for power apparatuses such as power transformers than what they originally have been designed for. The understanding of the magnetic losses under such load patterns, can allow for a controlled upgrading, including acceptance of short time overloads of existing transformers. Such operation outside the transformers' design specifications can greatly reduce the need for costly reinvestments in the power grid. On the other hand, higher loads lead inevitably to higher leakage flux, which can stress the transformers.

Laminated iron cores close to the windings are exposed to this leakage flux. Depending on the location, the leakage flux enters the core from different directions, going from being parallel to perpendicular to the lamination plane when going from inside the yoke window to outside the yoke. The leakage flux generates additional power losses [1], which can both influence the overall power loss level in the core and the local power loss, the latter with the risk of generating excessive heat close to the core surface, which can result in deterioration of the core insulation and degradation of the insulating oil. With the variable load situations arising, knowledge of the additional magnetic losses appearing due to stray flux becomes increasingly important.

The influence of the leakage flux on stray losses in the structural parts of transformers have been extensively studied [2]-[3]. For the magnetic core, the magnetic properties are measured in the rolling direction (RD) in the standardized specification [4]-[5]. While not yet standardized, 2-dimensional single sheet testing (SST) with various yoke configurations have been proposed [6]-[9]. Due to the limited area of uniform magnetization, the measurement does not allow for averaging of the properties over a large volume [6]. In addition to the investigation on the plane of a single sheet, loss measurements have been performed in lamination due to flux in the normal direction (ND) [10]-[12]. However, dedicated studies on the impact of the leakage flux on the core losses largely lack. As the leakage flux imposes onto lamination core in different channels [13] and with various phase [14], such studies should account both for the spatial loss distribution and different phase angles (i.e. resistive or inductive load conditions). In both standardized methods [4]-[5], the power loss is determined for flux densities with a single sinusoidal and unidirectional excitation. To study the magnetic loss in electrical sheets with the combined action of multi-directional flux, a measurement system based on the wattmeter method and the basic Epstein frame geometry was developed [15]. The system was designed to characterize the power loss due to ac magnetic flux densities in RD combined with flux densities in the transverse or normal direction. Additionally, the actual leakage configurations were emulated in the laminated core for the studies of the associated losses.

In this paper, we investigate the loss features under leakage flux entering the laminations and interacting with the main flux. The magnetic losses are measured for different flux magnitudes and orientations, and at varying phase angle between the leakage flux and the main flux. Additionally, the results are physically interpreted using finite element analysis.

II. Leakage Flux Configurations and Power Loss Characteristics

The orientation of the leakage flux inside a single-phase transformer is schematically demonstrated in Fig. 1. The directions where the leakage flux enters the laminated core lead to the following definitions:

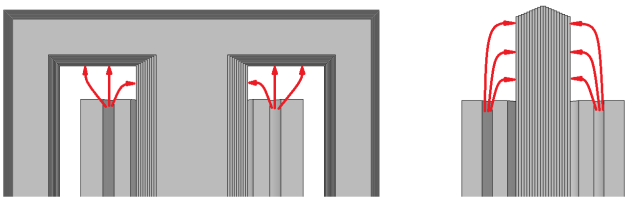

Fig. 1. Schematic drawing of the leakage flux at the top of the winding of a single-phase transformer. Left: TD; Right: ND.

1. **Transverse direction (TD)**: Below the yoke, the flux enters the core in parallel with the plane of the lamination and perpendicular to the rolling direction.

2. **Normal direction (ND)**: Ninety degrees outside the yoke, the flux enters the core perpendicular to both the plane of the lamination and the rolling direction.

The definition of the flux direction relative to a grain-oriented (GO) lamination block is illustrated in Fig. 2.

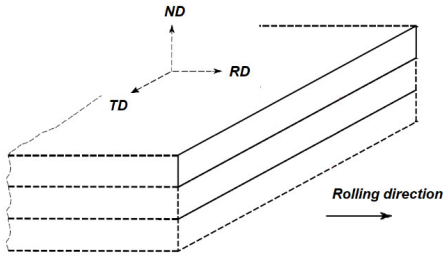

Fig. 2. Flux orientations in the grain-oriented steel laminations. RD: rolling direction; ND: normal direction; TD: transverse direction.

An example of leakage flux configuration is demonstrated in the simulation of a single-phase transformer (Fig. 3). The model is linear and no magnetic saturation is considered in the simulation. The high voltage (outer) winding sets up the main flux which circulates around the core window; the low voltage (inner) winding is connected to a load and the current in it sets up a balanced MMF. The leakage flux channel mainly locates between the two windings. Outside of the winding channel, the leakage flux entering the core (in either TD or ND) at the top of the transformer eventually turns and becomes parallel to the rolling direction before it again leaves the core at the bottom of the transformer. This flux path inside the core suggests two zones with different loss characteristics:

1. **Local zone:** Where the flux enters the core in either ND or TD, the flux orientation is maintained within a small depth in the core. The induced loss is associated with either eddy current loss (due to ND flux) [10]-[12] or rotational power loss (at TD flux) [6].
2. **Global zone:** As the entering flux changes direction and becomes parallel to the main flux (in RD), it follows the edge of the core window.

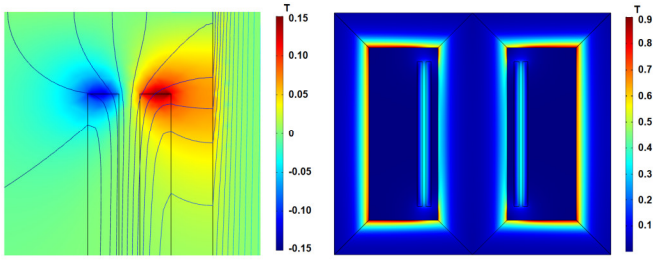

Fig. 3. Illustration of the local zone (left) and the global zone (right) of the leakage flux distribution in the core of a single-phase power transformer. Left: Leakage flux density component in *x*-axis (perpendicular to the limb). Right: Penetrated flux concentrated along the edge of the core window.

A transformer is operated under various loaded conditions. The magnitude of the secondary current I_2 depends on the secondary terminal voltage V_2 and the load impedance. The phase angle between I_2 and V_2 depends on the nature of the load. The load can be resistive, inductive or capacitive. The well-known schematic diagram of a loaded transformer at load condition is shown in Fig. 4.

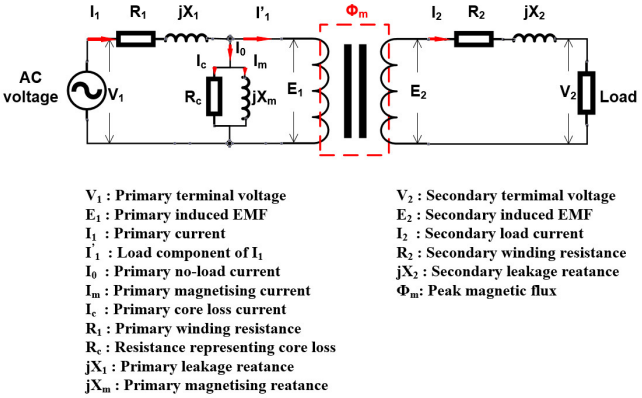

Fig. 4. Schematic diagram of a loaded transformer.

The primary no-load current I_0 induces the magnetomotive force (MMF) N_0I_0, which set up the flux Φ_m in the transformer core. Likewise, the secondary current I_2 induces the demagnetizing MMF N_2I_2 on the secondary winding of the transformer, setting up the counteracting flux Φ_2. N_1 and N_2 are the number of turns in the primary and secondary windings, respectively. An equilibrium is established when the primary current creates ampere-turns balance with the current of the secondary winding. The phasor diagrams of the actual transformer under resistive loading and inductive loading conditions are shown in Fig. 5.

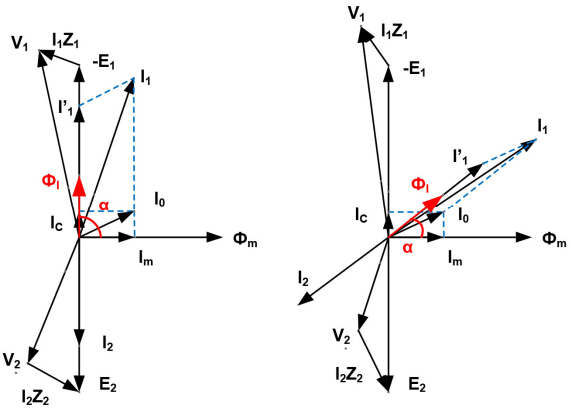

Fig. 5. The example of phasor diagram representing a loaded single-phase transformer. Left: resistive loading; Right: inductive loading.

The part of the flux produced by the primary winding, which does not link with the secondary winding, forms the leakage flux. The phase of the leakage flux Φ_l is in phase opposition with the load current. As shown, under resistive loading, the phase difference, α, between the core flux and the leakage flux is 90°, whereas under inductive load, α can decrease significantly depending on the phase of the load current. The phasor diagrams in Fig. 5 has demonstrated how load characteristic changes the phase difference between the main flux and the leakage flux. Therefore, the superimposition of the leakage flux and the main flux inside the transformer core is complicated not only by the directions, but also by the phase difference.

III. EXPERIMENT

As described in section II, the core losses not only depends on the main flux flowing in the rolling direction, but also influenced by the imposed multidirectional leakage flux. However, the standardized measurement methods [4]-[5] are insufficient to determine how different factors affect the power loss. To study the loss behavior with the combined action of main flux and leakage flux, a set of experiments were carried out. The experiments were organized in two parts: the reference measurement (III. B) was performed by using standardized measurement method (SST) for material characterization. The measurement results (magnetization curve and specific loss) provided the input for the later finite element analysis. The specific measurements for multidirectional flux (III. D and E) were performed based on the measurement system [15], which was designed to characterize the power loss due to ac magnetic flux densities in RD combined with flux densities in the transverse or normal direction.

A. Test samples

The strips to be tested (cold rolled grain oriented electric steel, Grade 30P120, JIS 2553 [16], Japan) were cut along the rolling direction (with angle tolerance of 1°), where the edge of the sheet defined the reference direction. The burr shall be <0.02 mm in specimen cutting. For unidirectional reference measurements, single strips (50 mm×150 mm) were used for single sheet tests (SSTs). For measurements in multi-directional flux, the sheets were cut into 30 mm×280 mm strips with 45° angle corner at both ends, and then assembled to form a frame [15] (see Fig. 8), similar to an Epstein frame, with mitered joints with the angle of overlap being 45°. The overall thickness of the lamination stack was 30 mm.

B. Reference measurements

To be used as a reference in the loss evaluation, the specific loss of the GO electrical steel was measured at 50 Hz as function of flux density according to the standard [5]. The losses were measured in the rolling direction (RD) and the transverse direction (TD) by means of single sheet tests (SSTs), see Fig. 6.

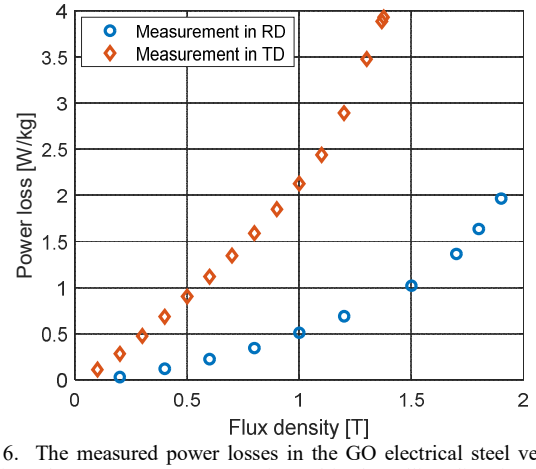

Fig. 6. The measured power losses in the GO electrical steel versus flux density. The measurement was performed in the rolling direction (RD) and the transverse direction (TD).

For the material definition to be used in the finite element analysis in Section IV, the magnetic permeabilities in two orthogonal directions up to the saturation level are obtained to account for the material anisotropy and the nonlinear effect [12]. The corresponding measurements were performed on the GO steel in RD and TD by SSTs. Two μ-B curves (μ_x-B_x curve for B_y=0 and μ_y-B_y curve for B_x=0) are shown in Fig. 7.

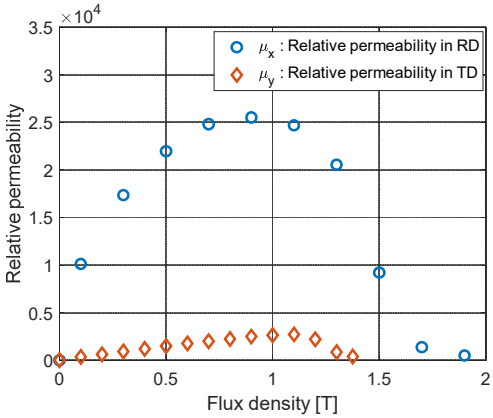

Fig. 7. The components of the permeability tensor versus flux density measured using the single sheet tester (SST). (μ_x: rolling direction, RD; μ_y: transverse direction, TD).

C. Loss measurement instrument for multidirectional flux

The measurement system developed for measurements of the losses under the combined action of RD and either TD or ND flux is described in detail in [15]. An overview of the system is given.

The main flux is generated in an Epstein-like frame with excitation coils and voltage pick-up coils, see Fig. 8. Each coil group had two concentric windings: an outermost primary winding (magnetizing winding), and an innermost secondary winding (voltage pick-up winding). A C-shaped powder core is used to produce an 'artificial leakage flux' (Fig. 9). The C-shaped core can be positioned such that it imposes the flux either in TD or ND.

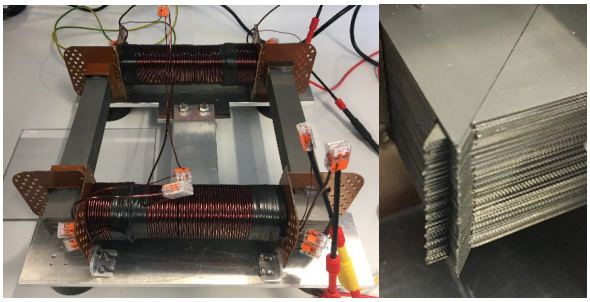

Fig. 8. The frame of the lamination sample with coils. The lamination frame and the coils formed the magnetic circuit. The frame comprised a sheet lamination with 103 layers, 30 mm in height. The individual primary and secondary windings of the two coils were connected in series. The mitered joints have a 5 mm offset and the angle of overlap was 45°.

The test object (Fig. 8) has two major differences comparing to a single-phase transformer (Fig. 1). First, the main flux circulates in the square frame instead of a core window. From flux distribution perspective, the Epstein-like frame is equivalent to a 'half' single-phase transformer.

However, the shape of steel strips used to build the frame is uniform and the complexity of assembly work is reduced. Moreover, for the material preparation and characterization, the standardized procedure [4] is available to follow.

Secondly, a C-shaped core is used to emulate leakage flux generated by the windings. Compared to the winding leakage flux, the artificial leakage flux has well defined incident areas, positions and directions, fully controllable magnitudes and phases of the flux densities. More importantly, by using specified leakage flux produced by the C-shaped core, the abovementioned factors can be studied independently. The detailed design parameters are listed in Table I.

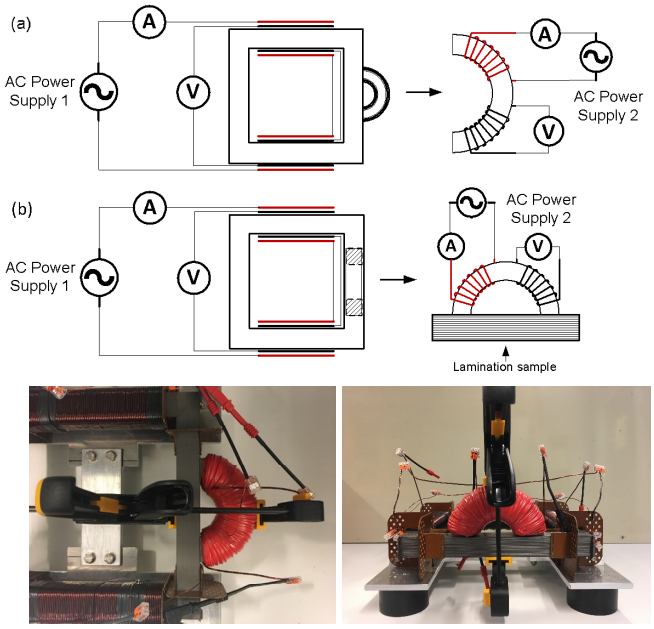

Fig. 9. The loss measurement system with artificial leakage flux superimposed with the main flux. The AC power supply 1 is connected to two coils wound around the square frame and the coil current generates the main flux in the frame. The AC power supply 2 is connected to a coil wound around the C-shaped core and the coil current generates the leakage flux to the lamination. The C-shaped core is mounted either on the side of the lamination (a) for TD flux or on the top of the lamination (b) for ND flux.

The measurement principle is based on the wattmeter method, where the primary current and secondary (induced) voltage are used to obtain the power loss. The secondary voltage $V_{2,rms}$ is calculated from the desired value of magnetic flux density B_{peak} by

$$V_{2,rms} = \sqrt{2}\pi f N_2 A B_{peak} \tag{1}$$

where N_2 is the total number of turns of the secondary winding and A is the cross-sectional area of the corresponding core. Since the secondary voltage contents only inductive voltage, the winding (resistive) loss is not involved in the measurement and thereby not sensitive to the temperature variation.

The net loss P_{net} (the total power loss subtracted by the loss in the powder core) of the test specimen and the incremental loss P_{incr} (the difference between the net loss P_{net} under superimposed flux and the arithmetic sum of the loss measured with individual excitation systems alone under unidirectional flux) due to flux superimposition are obtained.

$$P_{net} = \frac{N_1}{N_2}\tilde{P}_m + \frac{N_1^a}{N_2^a}\tilde{P}_m^a - P_{pow} \tag{2}$$

$$\begin{aligned} P_{incr} &= P_{net} - \left(\frac{N_1}{N_2}P_m + \frac{N_1^a}{N_2^a}P_m^a - P_{pow}\right) \\ &= \frac{N_1}{N_2}\left(\tilde{P}_m - P_m\right) + \frac{N_1^a}{N_2^a}\left(\tilde{P}_m^a - P_m^a\right) \end{aligned} \tag{3}$$

where $\tilde{P}_m$ and $\tilde{P}_m^a$ are the losses obtained from the wattmeter of the main excitation system (supplies the RD flux) and the auxiliary excitation system (i.e. the C-shaped core supplies the TD/ND flux) respectively [15]. The measurement is performed when both the lamination frame and the C-shaped core are excited simultaneously. In contrast, P_m and P_m^a are the losses of the main excitation system and the auxiliary excitation system measured individually. P_{pow} is the power loss of the C-shaped core, which needs to be measured according to [17] under specified flux densities and frequency prior to fabrication.

The phase difference between the artificial leakage flux and the main flux can be varied from 0° to 90°, which corresponds to from inductive to resistive loading of transformers.

TABLE I
PARAMETERS OF THE LAMINATION SAMPLE FRAME AND COILS

Parameters	Value	Unit
Total number of sheets	4×103	/
Total number of coils	2	/
Sheet width	30	mm
Sheet thickness	0.30±0.03	mm
Frame outer length	280±0.5	mm
Frame inner length	220±0.5	mm
Frame cross-section area	900	mm^2
Effective frame cross-section area	871	mm^2
Length of individual coils	190	mm
Number of turns, primary coil	2×100	/
Number of turns, secondary coil	2×100	/
Primary coil wire diameter	2	mm
Secondary coil wire diameter	1	mm

900 mm^2 is the geometric cross-sectional area.

D. Losses due to combined RD and TD magnetic flux

Loss measurements of the electrical steel were performed under the combined action of RD main flux and TD leakage flux at power frequency (50 Hz). The RD flux density (peak value) was set to 1.6 and 1.8 T. The TD flux was varied up to 0.6 T and was applied at different phase angles relative the RD flux.

The incremental loss (the total loss subtracted by the RD and TD loss measured individually) is given as function of phase angle in Fig. 10. The incremental loss increases with the magnitudes of the TD flux density as well as the RD flux density. The highest incremental loss occurs when the two fluxes are in phase, whereas the field components act practically independent of each other when the RD and TD fluxes are 90 degrees out of phase. This increment is predominated by the effect of the flux superimposition. As described in Section II, the flux inside the lamination is largely constituted by the one parallel to the RD. Therefore, a smaller phase difference results in a higher flux density and thereby higher power loss.

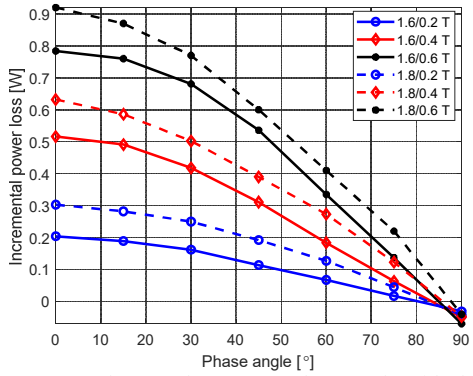

Fig. 10. Incremental power loss versus phase angle with the main flux superimposed with the transverse flux. The main flux densities are 1.6 T and 1.8 T; the transverse flux density varies from 0.2 T to 0.6 T.

E. Losses due to combined RD and ND magnetic flux

The power loss due to ND flux was measured at 50 Hz and 25 Hz and the flux density was varied from 0.2 T to 0.8 T, see Fig. 11. The power loss increases rapidly with the ND flux density and with frequency. This is due to the combined effect of the nonlinearity and anisotropy of the steel lamination, where the flux saturation extends the eddy current region and further increases the eddy current loss [12].

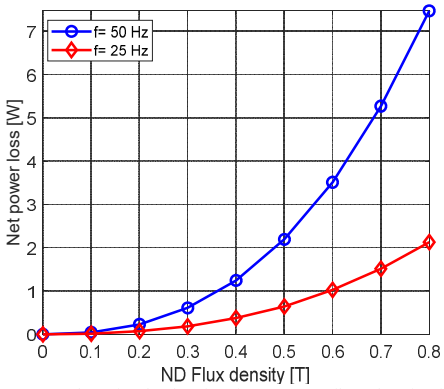

Fig. 11. Net power loss in the lamination versus flux density in the normal direction (without RD flux) at 25 and 50 Hz.

The measurement is further performed under the combined action of RD main flux and ND flux of varying phase angle. The frequency was 50 Hz, the RD flux density (peak value) was set to 1.6 T and the TD flux was either 0.2 or 0.4 T. The results are shown in Fig. 12.

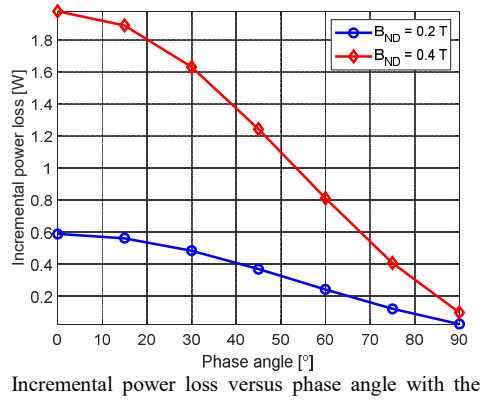

Fig. 12. Incremental power loss versus phase angle with the main flux superimposed with the normal flux. RD flux density B_{RD}=1.6 T; ND flux density and TD flux density are B_{ND}= 0.2 or 0.4 T.

Similar to the case of TD flux, the incremental loss induced by the ND flux increases as the phase difference between the two fluxes decreases. At the phase angle of 90 degrees, there is almost no difference in loss compared to the sum of the losses measured individually ND and TD flux.

However, comparing to the TD flux density of the same level, the ND flux produces much larger incremental loss and this incremental loss increases disproportionately to the magnitude of the ND flux density.

IV. Finite Element Analysis

A. Finite element model

The measured power losses consist of different types of losses, inseparable by the measurement results alone. To understand the physical phenomena of the experiment and to gain insight of the loss mechanisms associated with different flux configurations, the finite element (FE) models were developed. A two-dimensional (2D) FE model was developed to investigate the TD flux. Considering that the eddy current distribution is three-dimensional (3D), a 3D FE model was developed to investigate the ND flux. The geometry view of the 2D and 3D model is illustrated in Fig. 13.

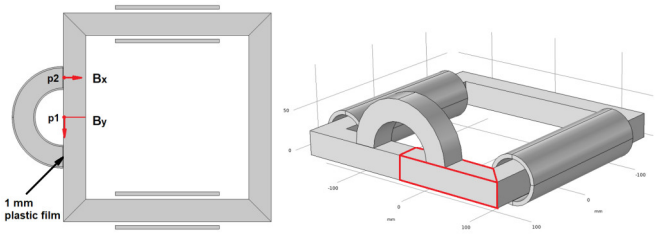

Fig. 13. The geometry view of the 2D and 3D models. Left: 2D model to study the TD flux and its flux superimposition with RD flux. Right: 3D model to study ND flux and its flux superimposition with RD flux.

The homogenization scheme is implemented in the material definition in the 3D finite element models [12] [18]. The equivalent relative permeability in the ND, μ_z is 30, determined by the stacking factor of the lamination and the equivalent conductivity in the ND, σ_z is 208 S/m, calculated based on the intrinsic conductivity of the electrical steel and the lamination geometry [19].

B. Simulation of TD flux combined with RD

Power losses measured in Section III.D consists of the loss contributed by the RD flux as well as the rotational field. The former is determined by the magnitude of the resultant RD flux density and the latter relies on both the RD flux and the TD flux. A numerical simulation was employed to calculate the two contributions separately.

Firstly, the flux density distribution in the lamination was examined. The simulation was made under unidirectional flux (without RD flux in the lamination frame) as well as under flux superimposition of varying phase angle. Figure 14 demonstrates the comparison of the flux distribution in the lamination with and without flux superimposition.

- With TD flux alone, the flux turns to become parallel to RD along the edge. Due to material anisotropy, the flux concentrates in a narrow flux channel and the magnitude of the RD flux density (0.67 T, B_y defined at P1 in Fig. 13) is larger than the incident ND flux density (0.2 T, B_x defined at P2 in Fig. 13).
- With RD flux alone, the flux distributes homogenously in the lamination frame with practically no flux flowing in the C-shaped core. However, when the permeability of the lamination steel is close to that of the C-shape core (heavy saturation), some flux could flow into the C-shaped core. To avoid this flux interaction, 1 mm plastic films (air gap) were positioned between the C-core and the main frame to isolate the flux (Fig. 13) [15].
- When superimposing TD flux in phase with the RD flux, B_y increases. As demonstrated in the B_y curve, the superimposition is not linear, i.e. the resultant flux density under flux superimposition is not the arithmetic sum of previous two fluxes. Instead, the saturation effect significantly extends the TD flux influence area (global zone). The combined effect of the increased magnitude of the RD flux density as well as the extended area contributes to the loss increment (Fig. 10).

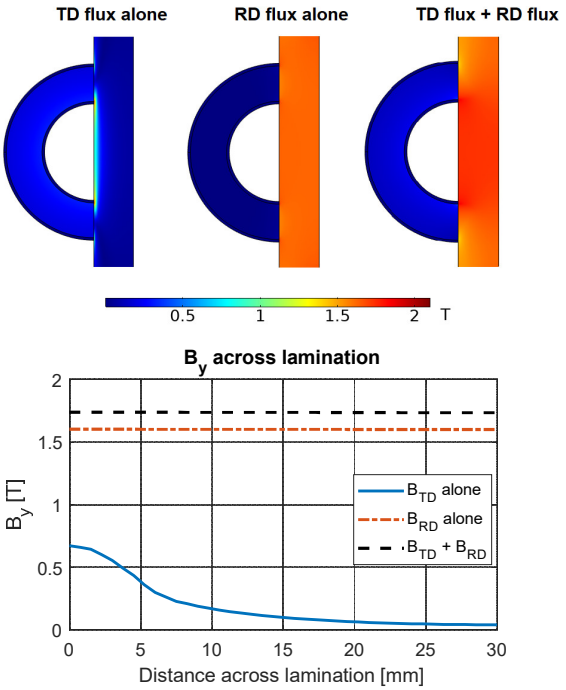

Fig. 14. Flux distribution in the steel lamination with incident TD alone (Left: B_{TD}=0.2 T; B_{RD}=0 T), RD alone (Middle: B_{TD}=0 T; B_{RD}=1.6 T) and with incident TD flux superimposed with RD flux (Right: B_{TD}=0.2 T; B_{RD}=1.6 T). The lower curve figure give the flux density in vertical direction By along the line in the middle of the lamination (red line in Fig. 13) corresponding to three scenarios in the upper figure.

Figure 15 demonstrates the flux density distribution in the horizontal direction. The contour of the B_x explicitly defines the 'local zone' associated with the TD flux as previously described in Fig. 5 (left). Apparently, the area of the local zone increases with a decreasing phase angle. At 90° phase angle, the area of the local zone is minimum. However, the area of the local zone is significantly smaller than the global zone, which indicates its relatively small loss contribution to the overall loss. This will be justified by the following calculation.

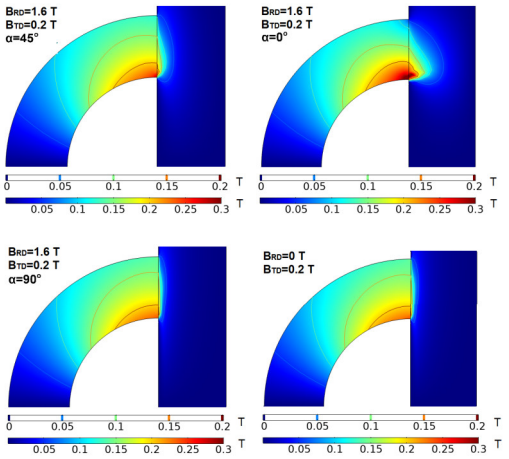

Fig. 15. Flux density in the horizontal direction B_x with incident TD flux superimposed with RD flux and with incident TD flux alone (lower right).

The power loss involving the rotational magnetic field can be estimated by the sum of the losses in two orthogonal directions [20]. Thereby, the total power loss is calculated by

$$P_{tot} = \int_V \left[P_x(\max_T(B_x)) + P_y(\max_T(B_y)) \right] dV \qquad (4)$$

where $P_x(B)$ and $P_y(B)$ are the specific loss density with respect to the peak flux density in TD and RD respectively. The reference specific loss [W/kg] measurement in two orthogonal directions (RD and TD) obtained by SST has been implemented in the finite element model. Considering the flux in two orthogonal directions not being always in phase (the peaks do not appear at the same time), the maximum value over a period shall be used.

The calculation example is given under TD flux density B_{TD}=0.2 T and RD flux density B_{RD}=1.6 T. As demonstrated in Table II, the power loss can be predicted accurately by (1). The calculation results gives an insight to the constitution of the measured power loss, which reveals that that the power loss is predominated by the RD flux and a decreased phase angle gives a rise on the resultant RD flux density, and thereby induces higher loss. On the contrary, the contribution from TD flux is small and can be ignored in practice.

TABLE II
NET POWER LOSS DUE TO TD FLUX COMBINED WITH RD FLUX

Phase angle [°]	Flux density at p1, B_y [T]	Net power loss in the core lamination [W]			
		Calculated			Measurement
		RD	TD	Total	/
0	1.737	8.923	0.0270	8.95	8.92
15	1.733	8.917	0.0268	8.94	8.91
30	1.726	8.906	0.0255	8.93	8.88
45	1.711	8.882	0.0229	8.90	8.83
60	1.672	8.810	0.0187	8.83	8.79
75	1.646	8.784	0.0152	8.80	8.74
90	1.607	8.677	0.0122	8.69	8.69

C. Simulation of ND flux combined with RD

Power losses induced by the ND flux consists of eddy current loss and hysteresis loss, where the latter is determined by the magnitude of the resultant RD flux density. The simulation is firstly made solely under ND flux (without flux superimposition). The calculation agrees very well with the measurement (see Fig. 16), showing that the eddy current constitutes the majority of the total power loss under ND flux. The small contribution from hysteresis loss explains why the measured power loss (in Fig. 11) has a frequency dependent factor less than the power of 2 (approximately 1.8).

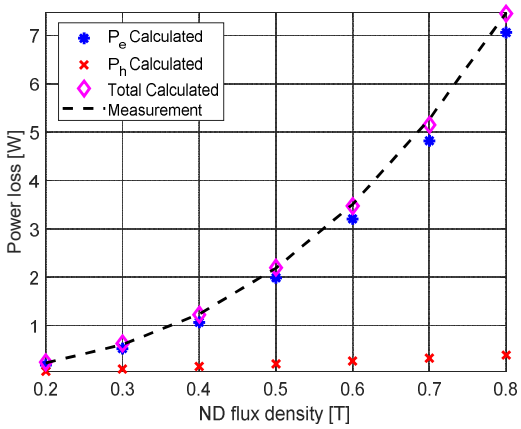

Fig. 16. The calculated power loss and the measured power loss under varying ND flux density. The calculated power loss has been separated by simulations, where P_e is the calculated eddy current loss and P_h is the calculated hysteresis loss.

With ND flux superimposed with RD flux, the distribution of the eddy currents has significantly changed and the phase difference between two fluxes plays a vital role in power loss enhancement. Fig. 17 shows the eddy current distribution under the flux superimposition between RD flux (1.6 T) and ND flux (0.2 T) at 90° and 0°, respectively.

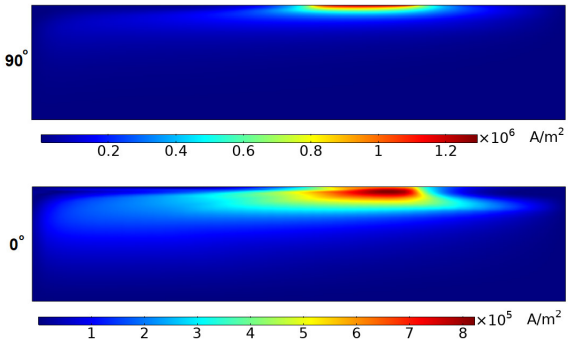

Fig. 17. The eddy current distribution in the lamination (red region highlighted in Fig. 13) under the ND flux (0.2 T) superimposed with the RD flux (1.6 T) at phase angle of 90° and 0°.

It is evident that the eddy current is concentrated close to the surface at 90° phase angle. In contrast, at 0° phase angle, the eddy current region is largely extended due to the saturation caused by flux superimposition. The extended eddy current volume leads to a significant loss increment, which explains the strong phase dependent eddy current loss shown in Fig. 12.

Under flux superimposition, the decreased phase angle also increases the hysteresis loss due to increased magnitude of the flux density, similar to the scenario discussed in Section III.B. As shown in Fig. 18, this incremental hysteresis loss can be comparable to the incremental eddy current loss. However, eddy current loss density is significantly larger than that of the hysteresis loss. More importantly, as the eddy current loss increases more rapidly with ND flux than the hysteresis loss, it becomes rather dominating (see Fig. 12) under higher ND flux density (0.4 T).

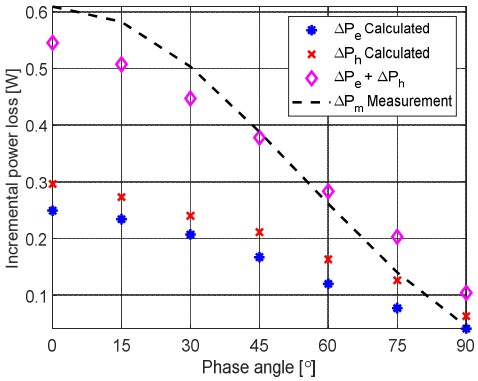

Fig. 18. The calculated incremental power loss and the measured incremental power loss under varying phase angle, ND flux density is 0.2 T and RD flux density is 1.6 T.

V. Discussion

Loss impact has been categorized into the local zone and the global zone in the core lamination, according the flux path and its orientation. The associated loss characteristic was investigated experimentally in Section III and numerically in Section IV.

A. Local zone

The leakage flux enters into the iron core perpendicularly to the core surface, either normal to the lamination plane or in the lamination plane but transverse to the rolling direction. Due to the leakage flux configuration and the material anisotropy, the penetrated flux is constrained within a small volume (Figs. 15 and 17) regardless the flux density and phase angle.

The induced loss associated with ND is eddy current loss and the induced loss associated with TD is the rotational power loss. Compared to the loss in the RD, the eddy current loss and the rotational loss produce much higher per volume loss (i.e. higher loss density), and can therefore lead to local hotspots. This has been confirmed experimentally in Section III.D and numerically in Section IVC, where the eddy current loss increases rapidly with the ND flux density (Fig. 11). More importantly, we found that the phase angle between the RD flux (main flux) and the ND flux also plays a significant role the eddy current enhancement (Fig. 12).

In literature [21], the influence of the homogenous TD flux on power loss has been investigated experimentally. It concludes that the TD flux can generate significant larger power loss than RD flux of the same level. However, we have demonstrated that, in a lamination structure, the TD flux is constrained within such a small volume (see Fig. 15) that the

associated rotational loss is rather insignificant compared to the eddy current loss induced by the ND flux (see Table II).

B. Global zone

The penetrated flux inside the core lamination is largely dominated by the flux parallel to the main flux (in RD), which circulates along the edge of the core window (Fig. 5, right). This flux path constitutes the global zone. Obviously, the influence region of the global zone is so much larger than the local zone that it has an impact on the overall core loss.

Since the flux involved in the global zone is in RD, the eddy current is limited by the lamination structure and the hysteresis loss dominates the power loss. The hysteresis loss hardly attribute to any local hot spot. Instead, it can considerably increase the overall power losses due to the larger volume it involves, particularly under inductive loading. In Fig. 10, taking the lowest TD flux density (0.2 T) as an example, the incremental loss is 0.2 W when it is in phase with the RD flux (1.6 T). This corresponds to 2.3% of the total frame loss. Considering the actual leakage flux has multiple exposures in a real transformer, the incremental loss could be substantial under inductive loading.

The incremental loss can be estimated based on the reference measurement on the laminated steels. The measured power loss is formulated in terms of Steinmetz's equation:

$$P_{est} = k_s B^n \tag{5}$$

where k_s is a material dependent constant (also incorporating constant frequency), B is the peak flux density, and n is the Steinmetz constant having a value of slightly more than 2.0 for cold rolled laminations [14]. As an approximation, 2.0 is used. Thus, the incremental loss ΔP_{est} can be expressed as:

$$\begin{aligned} \triangle P_{est} &= P_{net} - (\widetilde{P_m} + \widetilde{P_m^a}) \\ &= k_s \left(B_m + \triangle B\right)^2 - \left[k_s B_m{}^2 + k_s \left(\triangle B\right)^2\right] \end{aligned} \tag{6}$$

where B_m is the peak value of the initial main flux density; ΔB is the incremental flux density. Here, we assume the penetrated flux in the global zone concentrates in a channel with the width equal to the width of the exposure, and thereby the average flux density in the global zone equates the imposed TD leakage flux density B_l. This assumption leads to an under-estimation of the power loss, since the real flux density is inhomogeneous and the power loss is a convex function (see equation (5)) of flux density. Nevertheless, under this assumption, the incremental flux density ΔB can be simply expressed as B_l and the phase difference α between B_m and B_l:

$$\triangle B = B_l \cos\alpha \tag{7}$$

By inserting (7) into (6), we obtain:

$$\begin{aligned} \triangle P_{est} &= k_s \left(B_m + B_l \cos\alpha\right)^2 - k_s B_m{}^2 - k_s B_l^2 \\ &= k_s \left(2B_m B_l \cos\alpha + B_l^2 \cos^2\alpha - B_l^2\right) \end{aligned} \tag{8}$$

At a large phase angle ($\alpha \approx 90°$), the incremental loss becomes a small negative value:

$$\triangle P_{est} \approx -k_s B_l^2 \tag{9}$$

which can be observed in Fig. 10.

At a smaller phase angle ($\alpha \ll 90°$), the first term in (8) dominates, whereas the last two terms can be omitted, thus

$$\triangle P_{est} \approx 2k_s B_m B_l \cos\alpha \tag{10}$$

Equation (10) implies that the incremental loss is proportional to the main flux density B_m and B_l. This is in line with the measurement results shown in Fig. 10. Furthermore, we can calculate a percentage increase based on (10).

$$\frac{\triangle P_{est}}{P}\% \approx \frac{2k_s B_m B_l \cos\alpha}{k_s B_m^2}\% = \frac{2B_l \cos\alpha}{B_m}\% \tag{11}$$

$$\frac{\triangle P_{est}}{P}\% \overset{\alpha=0}{\approx} \frac{2B_l}{B_m}\% \tag{12}$$

Equation (11) and (12) can be used to estimate the loss percentage increase in the global zone due to flux superimposition. For example, the main flux density of 1.6 T superimposed with the leakage flux of 0.2 T leads to a 2×0.2/1.6=25% increase of power loss relative to the nominal condition (1.6 T) in the global zone. This corresponds to 2.2% of the total frame loss (considering volume ratio), which has a good agreement with the measurement (2.3%).

Little discrepancy at 90° phase angle (in Fig. 10) implies that the conventional no-load (unidirectional) test gives a good estimation on overall core loss in normal operation. However, underestimates the losses under inductive loading.

VI. Conclusions

The demonstrated combined experimental and numerical approach to determine the nature and importance of multidirectional leakage flux on the magnetic losses in transformer core lamination can be an effective tool for loss analyses.

The results show that the loading angle has a significant impact on the eddy current loss in the local zone as well as the overall power loss in the global zone of the transformer core. A smaller loading angle can aggravate the risk of local overheating and enhances the overall core losses. The conventional no-load test may underestimate magnetic core loss considerably under inductive loading due to ignorance of penetrated leakage flux.

In contrast, the rotational magnetic loss that appears locally has a negligible contribution, regardless of the phase and the magnitude of the superimposed leakage flux density.

Acknowledgment

This work was performed as a part of the project "Thermal Modelling of Transformers" (project number: 255178) funded by the Research Council of Norway, Statnett, Hafslund and Lyse Nett.

References

[1] M. Kozlowski and J. Turowski "Stray losses and local overheating hazard in transformers", CIGRE 1972, pp no. 12-10.

[2] Y. Liu et al, "Study of the Stray Losses Calculation in Structural Parts for HVDC Converter Transformers Based on the TEAM Problem 21 Family", *IEEE Transactions on Magnetics*, vol. 31, pp. 605-612, 2016.

[3] S. A. Mousavi, *Electromagnetic Modelling of Power Transformers for Study and Mitigation of Effects of GICs,* Ph.D. dissertation, Royal Institute of Technology, Stockholm, 2015, pp. 194-195.

[4] *Magnetic materials-Part 2: Methods of Measurement of the Magnetic Properties of Electrical Steel Strip and Sheet by Means of an Epstein Frame*, IEC 60404-2: 2008.
[5] *Magnetic materials-Part 3: Methods of Measurement of the Magnetic Properties of Electrical Steel Strip and Sheet by Means of a Single Sheet Tester,* IEC 60404-3: 2009.
[6] S. Zurek, *Characterisation of Soft Magnetic Materials Under Rotational Magnetisation*, 1st ed. CRC Press, London, 2018.
[7] M. Enokizono, T. Todaka, S. Kanao and J. Sievert, "Two-dimensional magnetic properties of silicon steel sheet subjected to a rotating field," *IEEE Transactions on Magnetics,* vol. 29, no. 6, pp. 3550-3552, Nov. 1993.
[8] M. Enokizono, T. Suzuki, J. Sievert, and J. Xu, "Rotational power loss ofsilicon steel sheet," *IEEE Transactions on Magnetics*, vol. 26, no. 5, pp. 2562–2564, Sep. 1990.
[9] T. Nakata, N. Takahashi, K. Fujiwara and M. Nakano, "Measurement of magnetic characteristics along arbitrary directions of grain-oriented silicon steel up to high flux densities," *IEEE Transactions on Magnetics*, vol. 29, no. 6, pp. 3544-3546, Nov. 1993.
[10] N. Hihat et al, "Experimental and Numerical Characterization of Magnetically Anisotropic Laminations in the Direction Normal to Their Surface", *IEEE Transactions on Magnetics*, vol. 47, pp. 4517-4522, 2011.
[11] T. Yagasiwa, Y. Takekoshi, and S.Wada, "Magnetics properties of laminated steel sheet for normal fluxes," *J. Magn. Magn. Mater.*, no. 26, pp. 340-342, 1982.
[12] W. Wang, A. Nysveen and N. Magnusson, "Eddy Current Loss in Grain-Oriented Steel Laminations Due to Normal Leakage Flux," in *IEEE Transactions on Magnetics*, vol. 57, no. 6, pp. 1-4, June 2021.
[13] D. Pavlik, D. C. Johnson and R. S. Girgis, "Calculation and reduction of stray and eddy losses in core-form transformers using a highly accurate finite element modelling technique," in *IEEE Transactions on Power Delivery*, vol. 8, no. 1, pp. 239-245, Jan. 1993.
[14] S. V. Kulkarni and S. A. Khaparde, *Transformer Engineering: Design and Practice*, 1st ed. Marcel Dekker, Inc., New York, pp. 42, 2004.
[15] W. Wang, A. Nysveen and N. Magnusson, "Apparatus for loss measurements under multidirectional and dc-bias flux in electrical steel laminations," *Rev. Sci. Instrument*. vol.91, Issue 8, 2020.
[16] *Cold-rolled grain-oriented electrical steel strip and sheet delivered in the fully processed state*, Japanese Industrial Standard. JIS C 2553: 2019.
[17] *Magnetic materials - Part 6: Methods of measurement of the magnetic properties of magnetically soft metallic and powder materials at frequencies in the range 20 Hz to 100 kHz by the use of ring specimens*, IEC 60404-6: 2018.
[18] J. P. A. Bastos and G. Quichaud, "3D modelling of a non-linear anisotropic lamination," *IEEE Transactions on Magnetics*, vol. 21, no 6, pp 2366-2369, November 1985.
[19] J. Wang, H. Lin, Y. Huang and X. Sun, "A New Formulation of Anisotropic Equivalent Conductivity in Laminations," *IEEE Transactions on Magnetics*, vol. 47, pp. 1378 -1381, 2011.
[20] H. Pfützner et al, "Rotational Magnetization in Transformer Cores-A Review", *Transactions on Magnetics*, vol. 47, no. 11, pp. 4523-4533, 2011.
[21] T. Kochmann, "Relationship between rotational and alternating losses in electrical steel sheets," *Journal of Magnetism and Magnetic Materials*, pp. 145-146, 1996.